

## A dual-color PAX7 and MYF5 *in vivo* reporter to investigate muscle stem cell heterogeneity in regeneration and aging

Sara Ancel,<sup>1,2,5</sup> Joris Michaud,<sup>1,5</sup> Federico Sizzano,<sup>3</sup> Loïc Tazuin,<sup>3</sup> Manuel Oliveira,<sup>1</sup> Eugenia Migliavacca,<sup>1</sup> Svenja C. Schüler,<sup>4</sup> Sruthi Raja,<sup>1</sup> Gabriele Dammone,<sup>1</sup> Sonia Karaz,<sup>1</sup> José L. Sánchez-García,<sup>1</sup> Sylviane Metairon,<sup>3</sup> Guillaume Jacot,<sup>1</sup> C. Florian Bentzinger,<sup>4</sup> Jérôme N. Feige,<sup>1,2,6,\*</sup> and Pascal Stuelsatz<sup>1,6,7,\*</sup>

<sup>1</sup>Nestlé Institute of Health Sciences, Nestlé Research, 1015 Lausanne, Switzerland

<sup>2</sup>School of Life Sciences, École Polytechnique Fédérale de Lausanne (EPFL), 1015 Lausanne, Switzerland

<sup>3</sup>Nestlé Institute of Food Safety & Analytical Sciences, Nestlé Research, 1015 Lausanne, Switzerland

<sup>4</sup>Département de pharmacologie-physiologie, Institut de pharmacologie de Sherbrooke, Centre de Recherche du Centre Hospitalier Universitaire de Sherbrooke, Faculté de médecine et des sciences de la santé, Université de Sherbrooke, Sherbrooke, QC J1H 5H3, Canada

<sup>5</sup>These authors contributed equally

<sup>6</sup>These authors contributed equally

<sup>7</sup>Lead contact

\*Correspondence: pascal.stuelsatz@rd.nestle.com (P.S.), jerome.feige@rd.nestle.com (J.N.F.)

<https://doi.org/10.1016/j.stemcr.2024.05.005>

### SUMMARY

Increasing evidence suggests that the muscle stem cell (MuSC) pool is heterogeneous. In particular, a rare subset of PAX7-positive MuSCs that has never expressed the myogenic regulatory factor MYF5 displays unique self-renewal and engraftment characteristics. However, the scarcity and limited availability of protein markers make the characterization of these cells challenging. Here, we describe the generation of StemRep reporter mice enabling the monitoring of PAX7 and MYF5 proteins based on equimolar levels of dual nuclear fluorescence. High levels of PAX7 protein and low levels of MYF5 delineate a deeply quiescent MuSC subpopulation with an increased capacity for asymmetric division and distinct dynamics of activation, proliferation, and commitment. Aging primarily reduces the MYF5<sup>Low</sup> MuSCs and skews the stem cell pool toward MYF5<sup>High</sup> cells with lower quiescence and self-renewal potential. Altogether, we establish the StemRep model as a versatile tool to study MuSC heterogeneity and broaden our understanding of mechanisms regulating MuSC quiescence and self-renewal in homeostatic, regenerating, and aged muscles.

### INTRODUCTION

Muscle stem cells (MuSCs) are tissue-resident stem cells that are essential for growth, maintenance, and repair of adult skeletal muscle throughout life (Bachman et al., 2018; Englund et al., 2020; Lepper et al., 2011; Sambasivan et al., 2011). Under homeostatic conditions, adult MuSCs reside in a quiescent state in a niche compartment located between the basal lamina and the muscle fiber plasma membrane (Dumont et al., 2015; Mauro, 1961; Schüler et al., 2022). The long-term regenerative potential of skeletal muscle relies on the ability of MuSCs to maintain, exit, and re-enter quiescence, a reversible cell-cycle-arrested state allowing cells to respond to different environmental signals (Ancel et al., 2021; van Velthoven and Rando, 2019). Age-associated regenerative failure of skeletal muscle is governed by defective cell-intrinsic mechanisms controlling features such as quiescence and activation, as well as by aberrant niche signals from the MuSC microenvironment (Ancel et al., 2021; Mashinchian et al., 2018; Sousa-Victor et al., 2022). Despite considerable recent success in characterizing these mechanisms, important unresolved questions about the balance of intrinsic and extrinsic signaling during aging and how it affects the stem cell pool remain (Ancel et al., 2021; Sousa-Victor et al., 2022).

MuSCs express the paired-box transcription factor PAX7, a canonical myogenic marker that represses genes involved in differentiation and is essential for proper muscle regeneration (Ancel et al., 2021; von Maltzahn et al., 2013; van Velthoven and Rando, 2019). Once they break quiescence, MuSCs upregulate myogenic regulatory factors (MRFs), a family of transcription factors associated with lineage progression and commitment to differentiation (Olguin and Olwin, 2004; Sambasivan et al., 2011; Seale et al., 2000). Activated MuSCs contain high levels of MYF5 and MYOD and subsequently progress toward terminal differentiation by downregulating PAX7, MYF5, and MYOD, while increasing the expression of Myogenin (MYOG) and MRF4 (Schmidt et al., 2019; Zammit, 2017).

Compelling evidence arising from the recent advent of single-cell profiling technologies has revealed an unexpected molecular heterogeneity of the MuSC pool. Some MuSC subsets show differential regulation of cell cycle progression, lineage commitment, self-renewal, repopulation of the niche, and the ability to resist environmental stress (Ancel et al., 2021). High PAX7 levels are associated with deeply quiescent MuSCs that are slower to enter the cell cycle, have lower metabolic activity, and have a greater ability to engraft in serial transplantations (Rocheteau et al., 2012). Similarly, expression of the surface markers CD34,



CD9, and CD104 has been linked to the differential capabilities of MuSCs to repopulate the niche after transplantation (Beauchamp et al., 2000; García-Prat et al., 2020; Porpiglia et al., 2017). *Pax3* expression has been associated with a subset of MuSCs in deeper quiescence that shows higher resistance and survival advantages in response to environmental stresses (Der Vartanian et al., 2019; Scaramozza et al., 2019). Apart from the downregulation of stemness genes involved in maintaining quiescence, commitment of MuSC subpopulations has been shown to depend on MRFs. In particular, MYF5 appears to play a central role in the epigenetic specification and commitment of MuSCs toward differentiation (Beauchamp et al., 2000; Kuang et al., 2007; McKinnell et al., 2008). Using *Myf5*-Cre; ROSA26-YFP mice, it has been demonstrated that MuSCs that are lineage negative for MYF5 self-renew through asymmetric divisions generating one committed daughter cell while maintaining a mother “satellite stem cell” (Kuang et al., 2007). MYF5 lineage-negative cells also show a higher engraftment and repopulation potential than lineage-positive cells. Supporting these findings, it has been shown that PAX7-positive MuSCs that are haploinsufficient for *Myf5* show an increased ability to self-renew and perform better in transplantation assays than wild-type controls (Gayraud-Morel et al., 2012). Altogether, these observations suggest that the stem cell pool in skeletal muscle is maintained by a MuSC subpopulation with superior stem cell characteristics. Importantly, given that aged skeletal muscle contains lower numbers of MuSCs (Sousa-Victor et al., 2022) and has an impaired regenerative capacity, it is conceivable that this stem cell subpopulation is particularly susceptible to the aging process.

Much of our current understanding of the MYF5-negative MuSC population is based on lineage tracing, which does not allow for conclusions regarding the real-time dynamics of this transcription factor in MuSCs. In addition, untranslated *Myf5* mRNA is sequestered into messenger ribonucleoprotein (mRNP) granules, making the prediction of protein levels using gene expression reporters challenging (Crist et al., 2012). Moreover, knockin reporter alleles such as the MYF5<sup>LacZ</sup> or MYF5<sup>GFP</sup> lines may be confounded by *Myf5* haploinsufficiency leading to altered MuSC function (Beauchamp et al., 2000; Kassar-Duchossoy et al., 2004; Tajbakhsh et al., 1996). Lastly, antibodies for the faithful detection of MYF5 protein in quiescent or activated MuSCs have been difficult to validate. For these reasons, the regulation of MYF5 protein in adult MuSCs and its potential implications in the aging process remain unclear.

To resolve this long-standing problem and study MYF5 protein levels in adult PAX7-positive MuSCs *in vivo*, we generated the StemRep dual-color reporter mouse line that links the last exon of the *Pax7* gene to an in-frame

T2A peptide and a nuclear-targeted zsGreen1 fluorescent protein. The same approach was used to connect nuclear-targeted far-red fluorescent E2Crimson to *Myf5*. In double-heterozygous StemRep mice, *Pax7* and *Myf5* are each expressed as a single transcript containing the uninterrupted coding frame linked to the nuclear-targeted fluorescent reporter proteins by T2A. Thus, post-translational cleavage of T2A in StemRep mice leads to the induction of dual nuclear fluorescence at equimolecular levels with MYF5 and PAX7 protein. Here, we demonstrate that the StemRep line allows for accurate *in vivo* assessment of MYF5 and PAX7 protein levels in MuSCs and enables efficient flow cytometry isolation and histological analysis of different stem cell subpopulations. We discovered that MuSCs containing high levels of PAX7 and low levels of MYF5 protein display sustained expression of canonical quiescence genes, show retention of PAX7 expression and a delay in MyoD induction after activation, are slower to enter the cell cycle, undergo asymmetric division, and have a lower capacity for clonal expansion. Aging induces a decline in the total number of PAX7-positive cells and skews the MuSC population toward a higher proportion of MYF5<sup>High</sup> cells. Altogether, StemRep mice represent a novel tool for the assessment of heterogeneity in the adult MuSC pool under different physiological conditions.

## RESULTS

### Generation and validation of StemRep mice

To produce dual PAX7 and MYF5 protein reporter (StemRep) mice, two separate transgenic lines were generated and later intercrossed. Briefly, a nuclear localization signal (NLS) fused to Zoanthus sp. green fluorescent protein (NLS-ZsGreen1) and the dsRed-derived E2Crimson far-red fluorescent protein (NLS-E2Crimson) was inserted in frame downstream of the last exon of *Pax7* and *Myf5* genes, preserving the entire coding region of both genes (Matz et al., 1999; Strack et al., 2009) (Figures 1A and 1B). Using this approach, *Pax7* and *Myf5* are co-translated with their respective fusion proteins to produce equimolar amounts of the reporter proteins. Both reporters were preceded by a self-cleaving T2A peptide sequence to induce post-translational separation of the reporter and generate an independent functional PAX7 or MYF5 protein. Successful targeting of both constructs was confirmed by PCR (Figure S1A), and double-homozygous StemRep mice were selected for subsequent applications based on greater signal-to-noise ratio of ZsGreen1 and E2Crimson fluorescence (Figure S1B). No apparent effects of the construct were observed on hindlimb muscle weight when StemRep mice were compared to wild-type animals at different ages (Figure S1C).

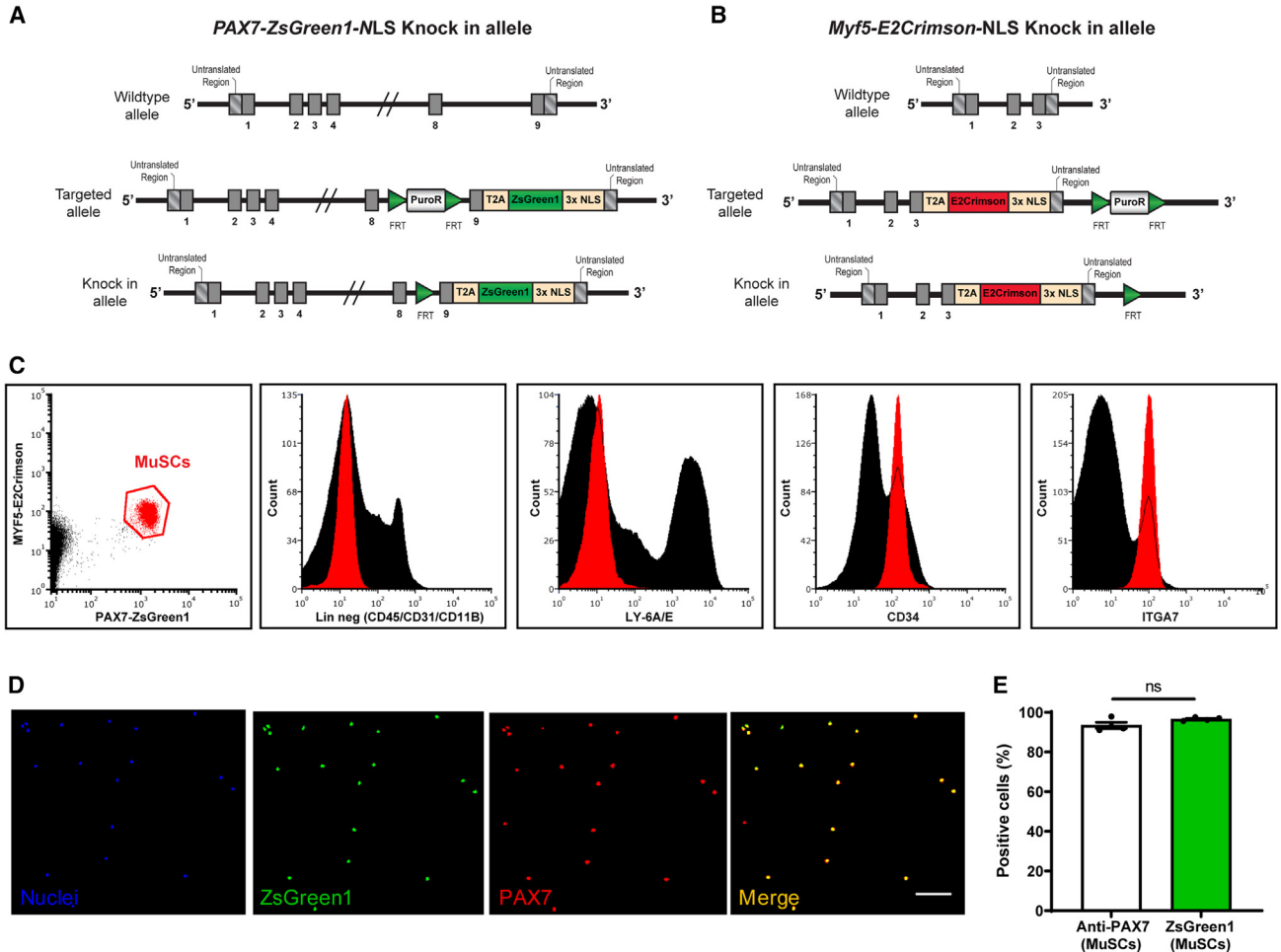


### Figure 1. Generation and characterization of StemRep mice

(A and B) Genetic constructs of (A) *Pax7-ZsGreen1-NLS* and (B) *Myf5-E2Crimson-NLS*. Representation of the wild-type allele (top), targeted allele (middle), and knockin allele after flippase-*FRT* recombination (bottom).

(C) Representative flow cytometry plots of MuSCs (red) derived from StemRep mice and the associated CD11b-/CD31-/CD45-/LY-6A/E-/CD34+/ITGA7+ antigen signature.

(D and E) Post-sort representative images of cytopsin preparations (D) and quantification (E) of MuSCs isolated based on nuclear ZsGreen1 fluorescence that stained positive using antibodies for PAX7. ZsGreen1 reporter, green; PAX7, red; Nuclei (Hoechst), blue. Scale bar, 50  $\mu$ m.  $n = 4$  mice. Data presented are means  $\pm$  SEM. ns = not significant in a two-tailed unpaired Student's *t* test (E).

We next analyzed the expression of MuSC-specific surface markers in ZsGreen1-positive cells of StemRep mice (Maesner et al., 2016). *PAX7-ZsGreen1* cells were negative for lineage markers (CD31, CD11b, CD45) and LY-6A/E (SCA1), but positive for CD34 and ITGA7, consistent with the expected surface antigen signature of MuSCs (Figures 1C and S1D). Conversely, all CD34 and ITGA7-positive MuSCs expressed *PAX7-ZsGreen1* (Figure S1E). Post-sort cytopsin analysis showed that the number of ZsGreen1-positive cells was not significantly different from cells identified by antibody staining for PAX7 (Figures 1D and 1E). To further confirm the specificity of the StemRep *Pax7* and *Myf5* dual reporter alleles in labeling

MuSCs, different muscles and tissues were analyzed by flow cytometry. While cells isolated from hindlimb, extraocular, and diaphragm muscles emitted in the ZsGreen1 and E2Crimson channels, no fluorescence was detected in either the brain, liver, or kidney (Figure S1F). Endogenous ZsGreen1 fluorescence and immunostaining of cryosections using dsRed antibodies against E2Crimson revealed robust nuclear fluorescence in the *tibialis anterior* (TA) of StemRep mice, while no signal was detected in the brain cortex, kidney, or liver (Figure S1G). Altogether, these data demonstrate that PAX7 and MYF5-dependent dual nuclear fluorescence in StemRep mice is specific to MuSCs.

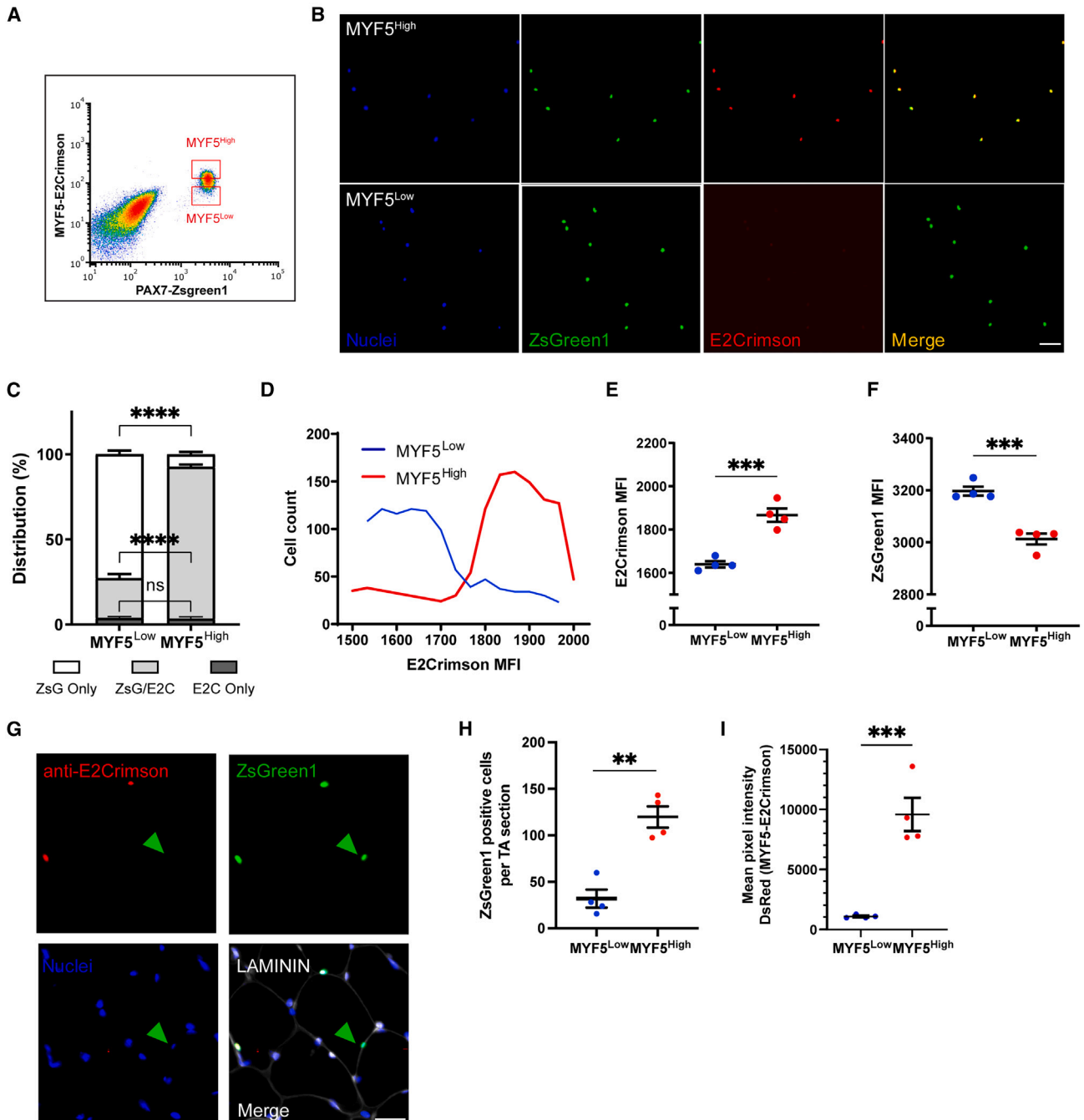


**Figure 2. Ex vivo and in vivo comparative characterization of MYF5<sup>High</sup> and MYF5<sup>Low</sup> MuSCs**

(A) Flow cytometry-based isolation strategy for MYF5<sup>High</sup> and MYF5<sup>Low</sup> MuSCs.

(B) Representative images of MYF5<sup>High</sup> and MYF5<sup>Low</sup> cells in cytospin preparations immediately after sorting. Scale bar, 100  $\mu$ m.

(C) Histogram showing the proportions of cells positive for either PAX7-ZsGreen1 or MYF5-E2Crimson, or both in isolated MYF5<sup>High</sup> and MYF5<sup>Low</sup> fractions.

(D) Distribution of MYF5<sup>High</sup> and MYF5<sup>Low</sup> cells according to E2Crimson intensity following isolation. A total of 1,000 cells per subpopulation were analyzed.

(E and F) Average intensity of E2Crimson (E) and ZsGreen1 (F) fluorescence in each subpopulation.

(G–I) Quantification of cells positive for PAX7-ZsGreen1 endogenous fluorescence and immunolabeled MYF5-E2Crimson on healthy muscle tissue sections. (G) Representative images and (H) quantification of the number of PAX7-ZsGreen1 and (I) of the mean intensity

(legend continued on next page)



To characterize MuSCs in StemRep mice, we isolated ZsGreen1-positive cells, cultured them in high-serum conditions, and live-imaged them every 12 h over a course of 4 days (Figures S2A–S2C) (Bentzinger et al., 2012). ZsGreen1-positive cells were able to differentiate and form elongated myocytes as their confluence increased (Figures S2A and S2B). This was accompanied by a progressive loss of *Pax7* expression as read-out by ZsGreen1 fluorescence (Figures S2A and S2C). In contrast to MYF5, validated antibodies that are able to faithfully detect PAX7 levels are readily available (Kawakami et al., 1997). Thus, to validate that nuclear ZsGreen1 correlates dynamically with the amount of PAX7 protein, we compared its fluorescent signal by immunostaining after MuSC isolation and downregulation in *ex vivo* culture over a time course of 7 days. PAX7 protein levels began to decline after 2 days in culture, which correlated directly with nuclear ZsGreen1 fluorescence, showing that the reporter allele closely recapitulates protein dynamics (Figures S2D, S2F, and S2G). E2Crimson antibody staining showed similar kinetics, suggesting that the fluorescent protein's half-life is not significantly longer than the one of ZsGreen1 or MYF5 (Figures S2E and S2H). Moreover, the downregulation of E2Crimson fluorescence correlated inversely with the differentiation marker Myogenin (Figures S2E and S2I). In parallel, we also tested the stability of the nuclear ZsGreen1 reporter following siRNA knockdown of *Pax7* (*siPax7*). Gray value quantification by western blot over a time course of 30 h revealed that after 12 h of knockdown, PAX7 and ZsGreen1 were downregulated to the same degree and continued to correlate until the experimental endpoint (Figures S2J and S2K). Altogether, these experiments demonstrate that both nuclear ZsGreen1 and E2Crimson have half-lives comparable to PAX7 and MYF5 and are well-suited fluorescent reporters to faithfully read-out endogenous protein levels.

#### MYF5-E2Crimson levels identify two subsets of MuSCs

Taking advantage of the StemRep model, we evaluated the capability of the E2Crimson reporter to discriminate MYF5 protein levels. Two MuSC subsets were isolated by fluorescence-activated cell sorting (FACS) at opposite ends of the E2Crimson spectrum and labeled as MYF5<sup>High</sup> and MYF5<sup>Low</sup> cells (Figure 2A). Re-analysis of sorted cells by flow cytometry confirmed that the isolated subpopulations consistently localized within the corresponding gates (Figures S3A and S3B). Fluorescence imaging after sorting

revealed that the majority of isolated MYF5<sup>Low</sup> cells were only positive for ZsGreen1 fluorescence (Figures 2B and 2C). In contrast, 93% of the sorted MYF5<sup>High</sup> population were positive for E2Crimson fluorescence with 90% also exhibiting ZsGreen1 fluorescence (Figures 2B and 2C). Average quantification of MYF5-E2Crimson fluorescence intensity in each population further verified that the gating strategy robustly discriminated MYF5 subpopulations (Figures 2D and 2E). We observed that ZsGreen1 fluorescence tracking PAX7 expression was higher in MYF5<sup>Low</sup> compared to MYF5<sup>High</sup> cells (Figure 2F). Because cell isolation by flow cytometry can alter the quiescent state of MuSCs (Machado et al., 2017; van Velthoven et al., 2017), we further validated that the MYF5 subpopulations are present in homeostatic muscles prior to isolation by quantifying the number of PAX7-ZsGreen1- and MYF5-E2Crimson-positive cells in histological cross-sections of muscles of StemRep mice. The *in vivo* MuSC population could be clustered based on MYF5-E2Crimson signal intensity in PAX7-ZsGreen1-positive cells with MYF5<sup>High</sup> and MYF5<sup>Low</sup> subpopulations discriminated with approximately 10-fold difference in E2Crimson signal intensity (Figures 2G–2I). In this setting, a MuSC population with undetectable levels of MYF5 could be identified and made up about 20% of PAX7-ZsGreen1-positive cells in adult muscle (Figures 2G and 2H), highlighting that MYF5 expression range is widespread in healthy quiescent MuSCs and that MYF5-negative MuSCs are rare *in vivo*. In summary, these data demonstrate that MYF5 protein is expressed in homeostatic muscle and that the MuSC pool is heterogeneous and contains a rare subset of PAX7<sup>High</sup> MYF5<sup>Low</sup> cells.

#### Functional heterogeneity of MYF5 subpopulations in StemRep mice

To assess the functional properties of MYF5<sup>High</sup> and MYF5<sup>Low</sup> MuSC subpopulations, isolated single clones were grown in high-serum conditions for 10 days (Figure 3A). No evidence of distinct clonal efficiency was observed, suggesting that the two populations are equally potent in starting a colony. However, colonies derived from MYF5<sup>High</sup> cells were on average larger (634 cells/clone) compared to the ones yielded by MYF5<sup>Low</sup> clones (489 cells/clone) (Figure 3B). We next analyzed the distribution of clones according to their size as well as their relative frequency. We found that 26% of MYF5<sup>Low</sup> colonies generated clones with less than 250 nuclei, while only 16% of MYF5<sup>High</sup> clusters fell into this category (Figure 3C). To

---

of immunolabeled E2Crimson (MYF5) signal on *tibialis anterior* cross-sections in uninjured muscle from StemRep mice. Scale bar, 50  $\mu$ m. The number of MuSCs *in vivo* was estimated by averaging all PAX7-ZsGreen1-positive cells from 2 complete muscle sections per mouse.  $n = 4$  mice. Data presented are means  $\pm$  SEM; \*\*\* $p < 0.001$ , \*\*\*\* $p < 0.0001$  in a two-tailed unpaired Student's t test (C, E, F, H, I).

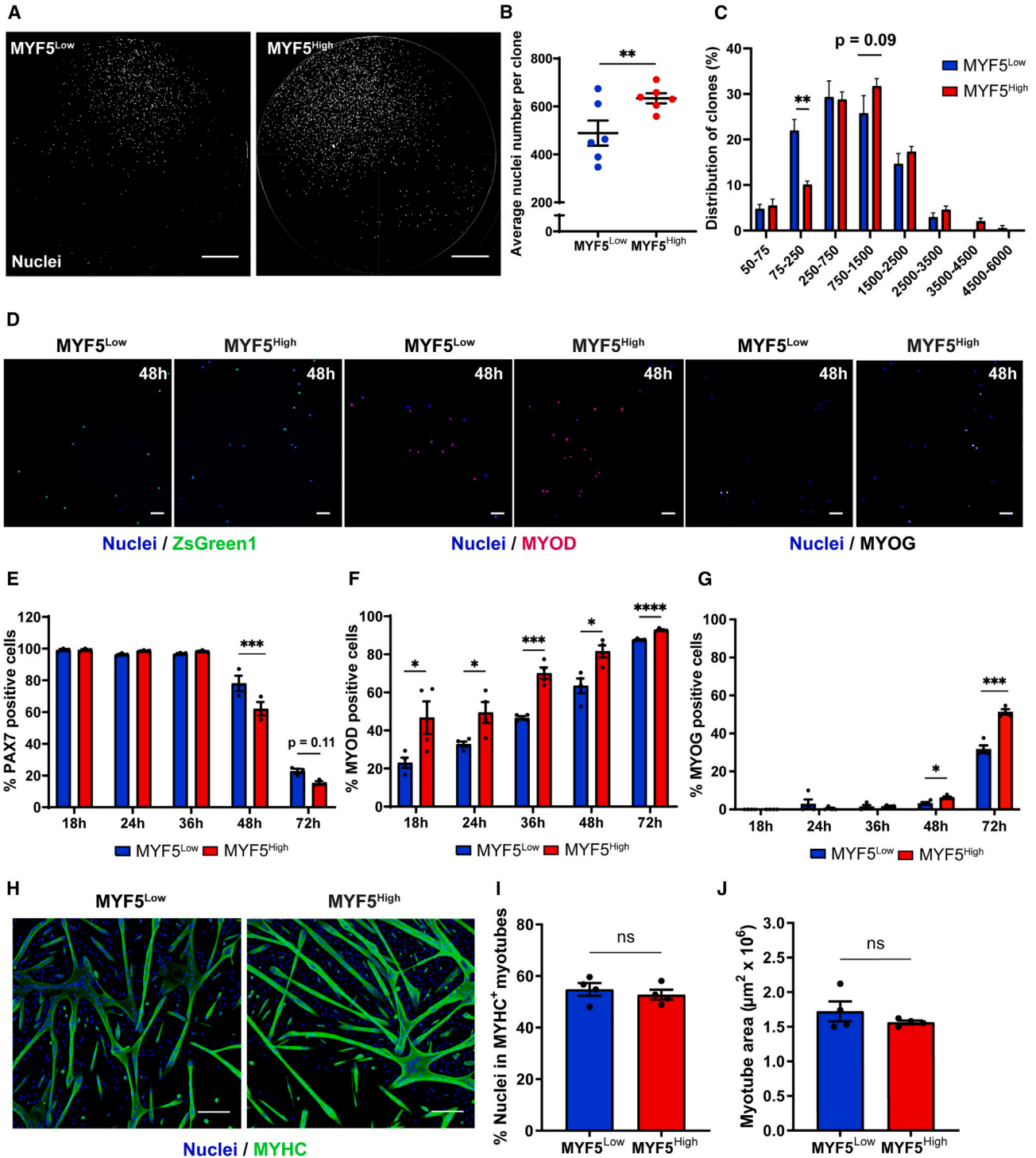


### Figure 3. Distinct clonal and functional properties of MYF5<sup>High</sup> and MYF5<sup>Low</sup> MuSCs

(A–C) Representative images (A), nuclei count (B), and size distribution of clones from freshly isolated MYF5<sup>High</sup> and MYF5<sup>Low</sup> cells after 10 days of culture (C).  $n = 6 \times 96$ -well plates from a pool of 4 mice. Scale bar, 1 mm.

(D) Representative pictures of PAX7, MYOD, and Myogenin expression in MYF5<sup>High</sup> and MYF5<sup>Low</sup> cells after 48 h of culture. Scale bars, 50  $\mu$ m.

(E–G) Quantification of PAX7 (E), MYOD (F), and Myogenin (G) over a 3-day time course.  $n = 4$  mice.

(legend continued on next page)



check if MYF5 subpopulations differed in terms of dynamics of myogenic progression, we interrogated the changes in protein levels of PAX7 and MYOD. By 48 and 72 h post-sort, 37% and 84% of MYF5<sup>High</sup> MuSCs downregulated PAX7, respectively, while 22% and 79% were negative in the MYF5<sup>Low</sup> condition at the respective time points (Figures 3D and 3E). Moreover, MYF5<sup>High</sup> MuSCs showed a 12%–49% higher induction of MYOD across the 3-day time course compared to MYF5<sup>Low</sup> cells (Figures 3D–3F). Finally, we evaluated differentiation kinetics between the two MYF5 fractions and observed that MYF5<sup>High</sup> cells upregulate MYOG earlier compared to MYF5<sup>Low</sup> cells (Figures 3D–3G). These results demonstrate that MYF5<sup>Low</sup> MuSCs are less committed to myogenic differentiation than MYF5<sup>High</sup> cells.

To assess the differentiation efficiency of the two MuSC subpopulations, MYF5<sup>Low</sup> and MYF5<sup>High</sup> cells were plated at confluence after isolation and the medium was changed to low-serum conditions the next day (Figure 3H). No significant changes were observed in terms of differentiation capacity based on the number of nuclei within myotubes and their total area (Figures 3I and 3J). These observations demonstrate that the differences between the two MuSC populations are constrained to the stem cell level and, once a differentiation signal is received, both cell types are equally potent in progressing through the myogenic program.

### MYF5<sup>Low</sup> MuSCs reside in deeper quiescence and have higher self-renewal capacity

To understand how underlying molecular mechanisms translate into distinct functional properties in MYF5 subpopulations, we performed RNA sequencing using freshly isolated MYF5<sup>Low</sup> and MYF5<sup>High</sup> MuSCs from adult StemRep mice. For the first time in this study, we observed sex differences in this experiment. Principal component analysis of all expressed genes revealed a separation according to male and female mice that accounted for 30% of the total variance, while MYF5 expression accounted for 19.9% (Figure 4A). When examining sex-independent gene signature differences between the MuSC populations, we observed an enrichment in transcripts related to activation and differentiation in the MYF5<sup>High</sup> fraction (Figures 4B–4D). Supporting the notion that MYF5 levels control the exit from quiescence and activation, when equal numbers of freshly isolated MuSCs from StemRep mice were plated in pro-proliferative media, the nuclei count in the

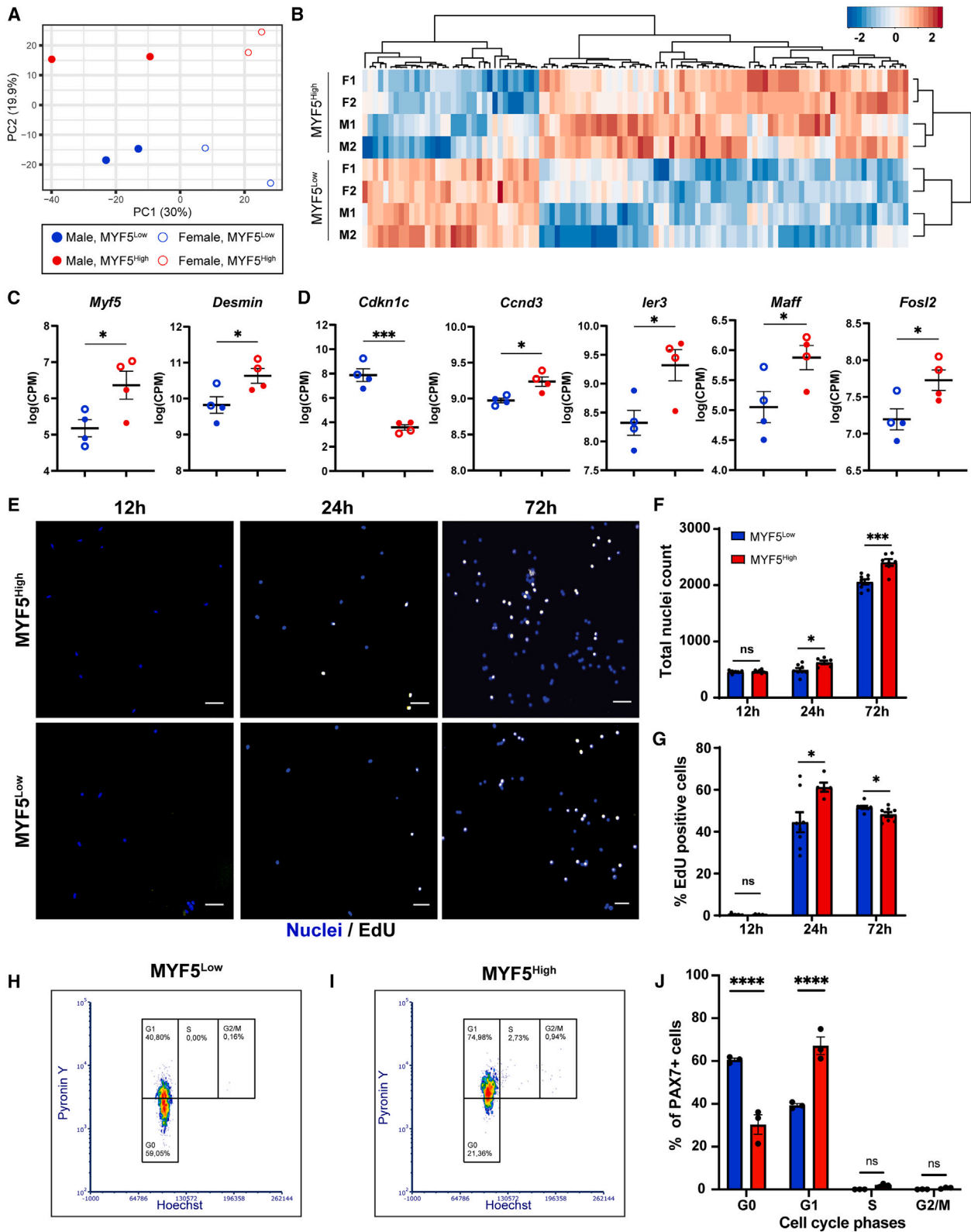
MYF5<sup>Low</sup> condition was 21% lower at 24 h and 14% lower at 72 h when compared to MYF5<sup>High</sup> cells (Figures 4E and 4F). Confirming slower activation under pro-proliferative conditions, 16% fewer MYF5<sup>Low</sup> MuSCs incorporated EdU at 24 h when compared to the MYF5<sup>High</sup> condition (Figure 4G). Finally, cell cycle analysis showed that most MYF5<sup>Low</sup> MuSCs (59%) were still in G0 after isolation (Figures 4H–4J and S4A–S4C). On the other hand, only 21% of MYF5<sup>High</sup> MuSCs were found in G0, whereas the vast majority (75%) had already transitioned into G1 (Figures 4I, 4J, and S4A–S4C). Collectively, these results demonstrate that MYF5<sup>Low</sup> MuSCs in StemRep mice activate slower than MYF5<sup>High</sup> cells.

MuSCs maintain their stemness throughout life via a tightly regulated control of the balance of quiescence and the ability to self-renew during cell division (Ancel et al., 2021). To evaluate whether the MYF5 MuSC subpopulations reside in different states of quiescence, we performed qPCR for several validated markers (Fukada et al., 2007; van Velthoven and Rando, 2019). Notably, all quiescence markers assessed were significantly enriched in the MYF5<sup>Low</sup> fraction compared to MYF5<sup>High</sup> MuSCs (Figures 5A–5D). We next evaluated whether MYF5<sup>Low</sup> and MYF5<sup>High</sup> MuSCs show differential self-renewal capabilities using an *ex vivo* assessment of the asymmetric segregation of MYOD in cell doublets in the two MYF5 subpopulations during the first round of division between 18 and 36 h post-sort (Figures 5E–5G). At both time points, the majority of MYF5<sup>High</sup> MuSCs underwent symmetric divisions while MYF5<sup>Low</sup> MuSCs showed almost exclusively asymmetric MYOD segregation into daughter cells (Figures 5E–5G). Overall, these results demonstrate that the rare MYF5<sup>Low</sup> MuSC subpopulation resides in deeper quiescence and exhibits more robust asymmetric division to enable self-renewal compared to MYF5<sup>High</sup> cells.

### *In vivo* dynamics of MYF5 subpopulations during muscle regeneration

Because of the central role of MuSCs in skeletal muscle regeneration, we capitalized on the StemRep model to dynamically monitor MYF5 subpopulations at different stages after activation *in vivo*. MuSCs were isolated after cardiotoxin injury and analyzed at different time points by flow cytometry. Consistent with a downregulation of both PAX7 and MYF5 during myogenic progression at early time points after injury (Bentzinger et al., 2012; Schmidt et al., 2019), the fluorescence intensity of both reporters

(H–J) Representative pictures (H) and quantification of fusion capacity (I) and myotube size (J) of MYF5 subpopulations. Myotube area was defined as the area positive for the myosin heavy chain (MyHC). Scale bar, 100  $\mu$ m.  $n = 4$  mice. Data presented are means  $\pm$  SEM; \* $p < 0.05$ , \*\* $p < 0.01$ , \*\*\* $p < 0.001$ , \*\*\*\* $p < 0.0001$  in a two-tailed unpaired Student's *t* test for each condition and/or time point (B, C, D, E, F, G, I, J).



(legend on next page)



at 3 and 7 days post injury (dpi) markedly decreased (Figures 6A, 6B, and S5). ZsGreen1 and E2Crimson fluorescence was progressively restored to basal levels as MuSCs re-entered quiescence after repair in later stages at 14 and 21 dpi. Immunostaining quantification using ZsGreen1 endogenous fluorescence and dsRed antibody against E2Crimson showed that the number of myogenic progenitors increased over 20-fold at 3 dpi before returning to homeostatic levels around 21 dpi (Figure 6C). PAX7<sup>High</sup> MYF5<sup>Low</sup> MuSCs were detectable throughout all stages of skeletal muscle regeneration on muscle sections (Figure 6D). These data demonstrate that StemRep mice allow to monitor PAX7- and MYF5-based heterogeneity in the MuSCs pool during regeneration *in situ*.

### Aging specifically reduces MYF5<sup>Low</sup> cells and skews the MuSC pool toward MYF5<sup>High</sup> cells

StemRep mice developed the expected *bona fide* skeletal muscle wasting phenotypes during aging, with muscle fiber size distribution in old 24-month-old (m.o.) StemRep mice shifting toward smaller myofibers and 17% reduction in average fiber area compared to 4 m.o. adult controls (Figures S6A and S6B). To study how MYF5 protein levels in MuSCs are regulated during the aging process, we evaluated their fluorescence profile in hindlimb muscles of adult and aged mice by flow cytometry (Figure 7A). Compared to 4 m.o. adult mice with a predominantly quiescent MuSC pool, aged 24 m.o. muscles contained fewer MuSCs (Figures 7A and 7B) and displayed a 13% increase in E2Crimson mean fluorescence intensity across the entire stem cell population (Figures 7A–7C). In line with the assumption that the maintenance of uncommitted MuSCs is impaired with aging, the MYF5<sup>High</sup> population became more abundant in 24 m.o. StemRep mice (Figures 7D, 7E, S6C, and S6D). To confirm our flow cytometry analysis histologically, we quantified the number of PAX7-ZsGreen1 and MYF5-E2Crimson cells in muscle cross-sections of adult and aged StemRep mice. This experiment revealed that aging of StemRep mice reduced the amount of PAX7-ZsGreen1-positive cells by 26% (Figure 7F) and skewed the distribution of MYF5 MuSC subpopulations with a reduced proportion MYF5<sup>Low</sup> but not MYF5<sup>High</sup> cells when compared

to adult controls (Figures 7G–7I). These changes in proportion translated to a 74% decrease of the absolute number of MYF5<sup>Low</sup> cells in aged muscle (Figure 7J), without significant changes of MYF5<sup>High</sup> cells (Figure 7K), demonstrating that aging affects specifically the MYF5<sup>Low</sup> population with higher quiescence. Altogether, these data support the notion that aging affects the MuSC pool by reducing the number of self-renewing PAX7<sup>High</sup> MYF5<sup>Low</sup> cells, which results in exit from quiescence and a higher propensity to activate and commit to differentiation.

## DISCUSSION

Diverse post-transcriptional mechanisms regulating mRNA stability, storage, and the rate of translation have been discovered (Shyu et al., 2008). In particular, stem cell populations that remain quiescent over much of their lifetime are able to store mRNA allowing them to be primed for efficient activation (Cheung and Rando, 2013). These considerations are particularly important with respect to the regulation of MYF5, which has been shown to be a key factor for MuSC commitment. In quiescent MuSCs, the mRNA coding for MYF5 and microRNA-31 suppressing its translation have been shown to be stored in mRNP granules (Crist et al., 2012). Once the cells activate, mRNP granules in MuSCs dissolve and miR-31 levels are lowered leading to an accumulation of MYF5 protein. In the earliest stages of MuSC activation, this process has been suggested to be independent of transcription. Another mechanism uncoupling mRNA from protein levels in quiescent MuSCs involves the translation initiation factor eIF2 $\alpha$  (Zismanov et al., 2016). eIF2 $\alpha$  is phosphorylated by PKR-like endoplasmic reticulum kinase leading to a general downregulation of global translation and selectivity toward certain mRNAs. In addition, phosphorylated eIF2 $\alpha$  is required for the formation and maintenance of mRNP granules containing MYF5 and MYOD. Therefore, knockin reporter alleles for MYF5 such as MYF5<sup>LacZ</sup> or MYF5<sup>GFP</sup> provide valuable insights into gene regulation, but make it difficult to predict protein levels accurately (Beauchamp et al., 2000; Kassar-Duchossoy et al., 2004; Tajbakhsh et al., 1996).

### Figure 4. MYF5<sup>Low</sup> MuSCs activate slower than MYF5<sup>High</sup> cells

(A) Principal component analysis of MYF5<sup>High</sup> and MYF5<sup>Low</sup> MuSCs isolated from male and female StemRep mice. Each datapoint represents 50,000 MuSCs isolated from a pool of 4 animals.  
(B) Heatmap of differentially expressed genes between the MYF5<sup>High</sup> and MYF5<sup>Low</sup> transcriptomes.  
(C and D) Differential expression of selected muscle- (C) and cell cycle-related genes (D) between MYF5 fractions in the male datasets.  
(E–G) Representative images (E) and quantification of nuclei (F) and EdU-positive cells (G) in MYF5<sup>High</sup> and MYF5<sup>Low</sup> subpopulations over a 3-day time course.  
(H–J) Cell cycle analysis of MYF5<sup>Low</sup> (H) and MYF5<sup>High</sup> (I) populations by flow cytometry and corresponding quantification of cell proportion within each cell cycle phase (J). Scale bar, 50  $\mu$ m.  $n = 4$  mice. Data represent means  $\pm$  SEM; \* $p < 0.05$ , \*\*\* $p < 0.001$ , \*\*\*\* $p < 0.0001$  in a two-tailed unpaired Student's  $t$  test for each condition and/or time point (C, D, F, G, J).

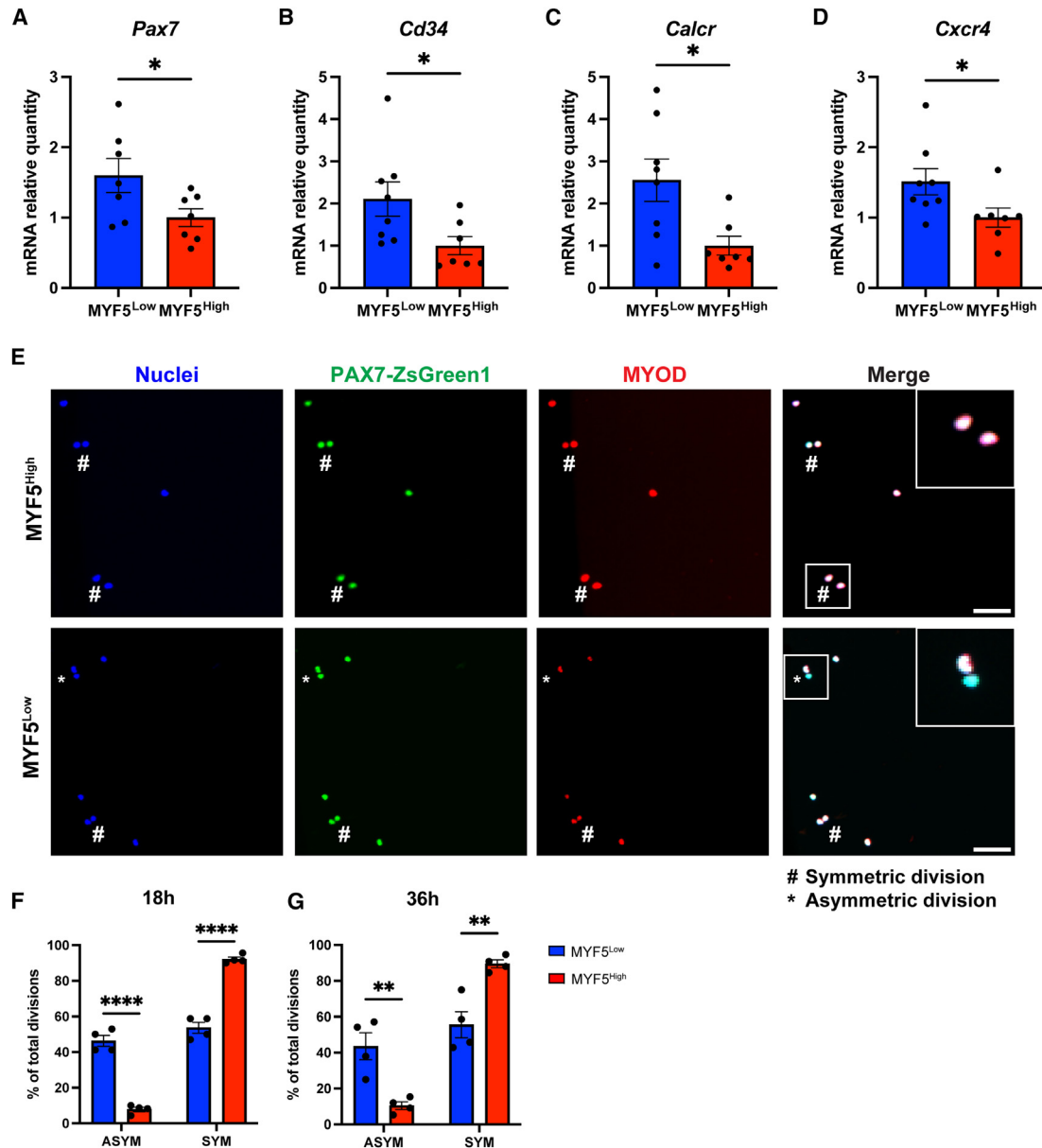


**Figure 5.** MYF5<sup>Low</sup> cells are deeply quiescent and exhibit increased self-renewal compared to MYF5<sup>High</sup> cells *ex vivo*

(A–D) qPCR of canonical quiescence genes in MYF5 subpopulations. *n* = 8 mice.

(E–G) Representative images at 36 h (E) and *ex vivo* quantification at 18 h (F) and 36 h (G) post-sort of asymmetric segregation of MYOD in MYF5 cells. Scale bar, 50 μm. *n* = 4 mice. Data represent means ± SEM; \**p* < 0.05, \*\**p* < 0.01, \*\*\*\**p* < 0.0001 in a two-tailed unpaired Student's *t* test for each population (A, B, C, D, F, G).

Depending on the targeting strategy, such alleles can also result in haploinsufficiency accompanied by a partial loss of gene product (Morrill and Amon, 2019). Thus, gene-dosage-dependent effects are yet another aspect that needs to be considered when analyzing stem cell function in knockin reporter models.

Raising antibodies to a protein of interest can help determine and study its function. However, this approach is not

always successful, and off-target reactivity as well as high levels of background signal are often a problem. As an alternative, epitope tagging, for instance using fluorescent proteins, is a frequently employed strategy to characterize, purify, and determine the *in vivo* localization of gene products (Brizzard, 2008). A limiting aspect of epitope tags is their potential interference with protein structure and function. The recent discovery of “self-cleaving” 2A peptides that are

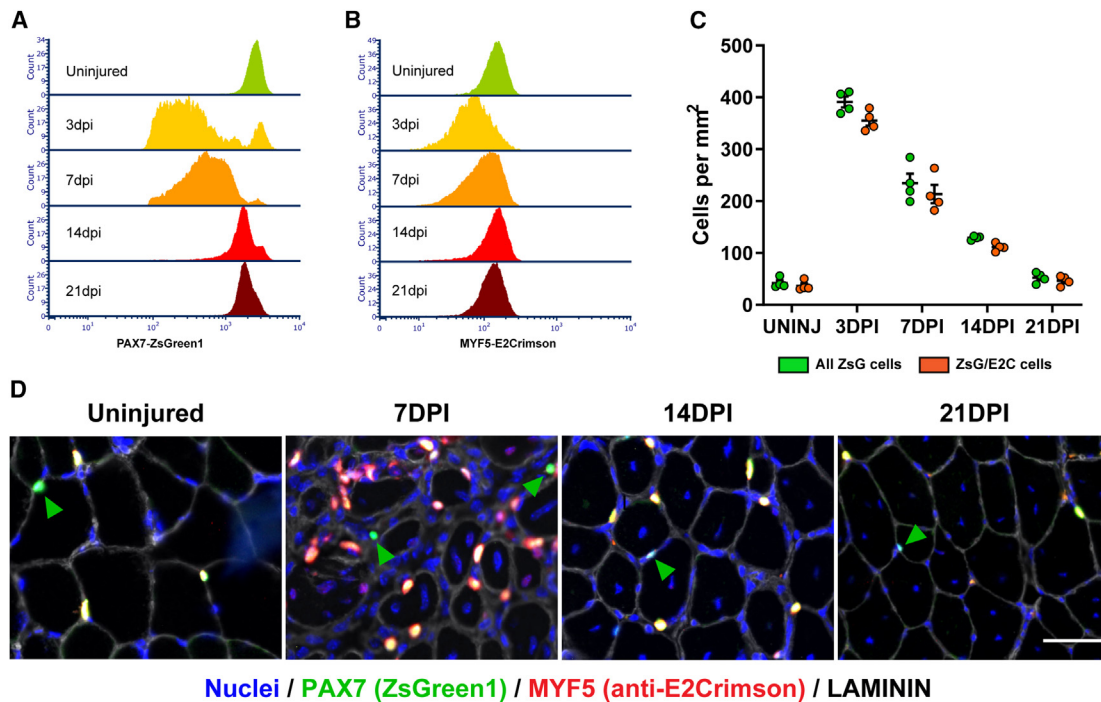


**Figure 6. Characterization of MYF5<sup>High</sup> and MYF5<sup>Low</sup> MuSC subpopulations during muscle regeneration**

(A and B) Flow cytometry analysis of PAX7-ZsGreen1 (A) and MYF5-E2Crimson (B) fluorescence intensity dynamics in MuSCs isolated from quadriceps under uninjured conditions and at 3, 7, 14, and 21 dpi.

(C and D) Quantification (C) and representative images (D) of MuSC subpopulations from tibialis anterior histological cross-sections at multiple stages of regeneration. Scale bar, 50  $\mu\text{m}$ .  $n = 4$  mice per group, each datapoint represents one mouse. Data presented are means  $\pm$  SEM.

present in a wide range of viral families has allowed to partially bypass this problem (Liu et al., 2017). 2A-mediated self-cleavage has been suggested to involve a failure of the ribosome in making a peptide bond (Liu et al., 2017; Luke et al., 2008). Therefore, 2A peptides can be used to link a genomic locus of interest to post-translationally cleaved epitopes leaving protein function unimpaired and resulting in equimolar levels of gene product and reporter. While subcellular localization is difficult to analyze using this strategy, it is well suited to measure the amount of a given protein product across cell populations. Importantly, when quantitative assessment of a gene product based on a reporter molecule is attempted, 2A peptides have the advantage that they do not suffer from lower expression levels of downstream proteins occurring in bicistronic mRNA open reading frames with internal ribosomal entry site elements (Hennecke et al., 2001). Next to P2A derived from porcine teschovirus-1 2A, the T2A peptide derived from *Thosea asigna virus* 2A has been shown to have particularly high cleavage efficiency in mammalian cells (Donnelly et al., 2001; Kim et al., 2011; Szymczak et al., 2004). Here, we used T2A to link the last exon of the *Pax7* and *Myf5* genes to two different nuclear-targeted

fluorescent proteins, allowing for assessment of the dynamics of these two factors on the protein level *in vivo* and after isolation *in vitro*. NLSs are short peptides that mediate the translocation of proteins from the cytoplasm into the nucleus (Mahato et al., 1999). MuSC numbers and function are often analyzed using thin skeletal muscle cross-sections. Due to their two-dimensional nature, it is challenging to quantify the confines of cells marked by cytoplasmic or membrane proteins in this type of sample preparation. The addition of NLS to the reporter proteins in StemRep mice has solved this problem and allows for convenient identification, quantification, and isolation of MuSCs with different levels of PAX7 and MYF5. Thus, the StemRep model will facilitate the study of MuSC heterogeneity under different physiological and pathological conditions.

Using StemRep mice, we confirmed that all cells expressing the canonical MuSC cell surface markers  $\alpha 7$ -integrin and CD34 were positive for PAX7-ZsGreen1 fluorescence. Live-cell imaging, muscle regeneration after experimental injury, and flow cytometry analysis at different ages confirmed that PAX7-ZsGreen1 and MYF5-E2Crimson reporters are dynamically regulated and faithfully recapitulate

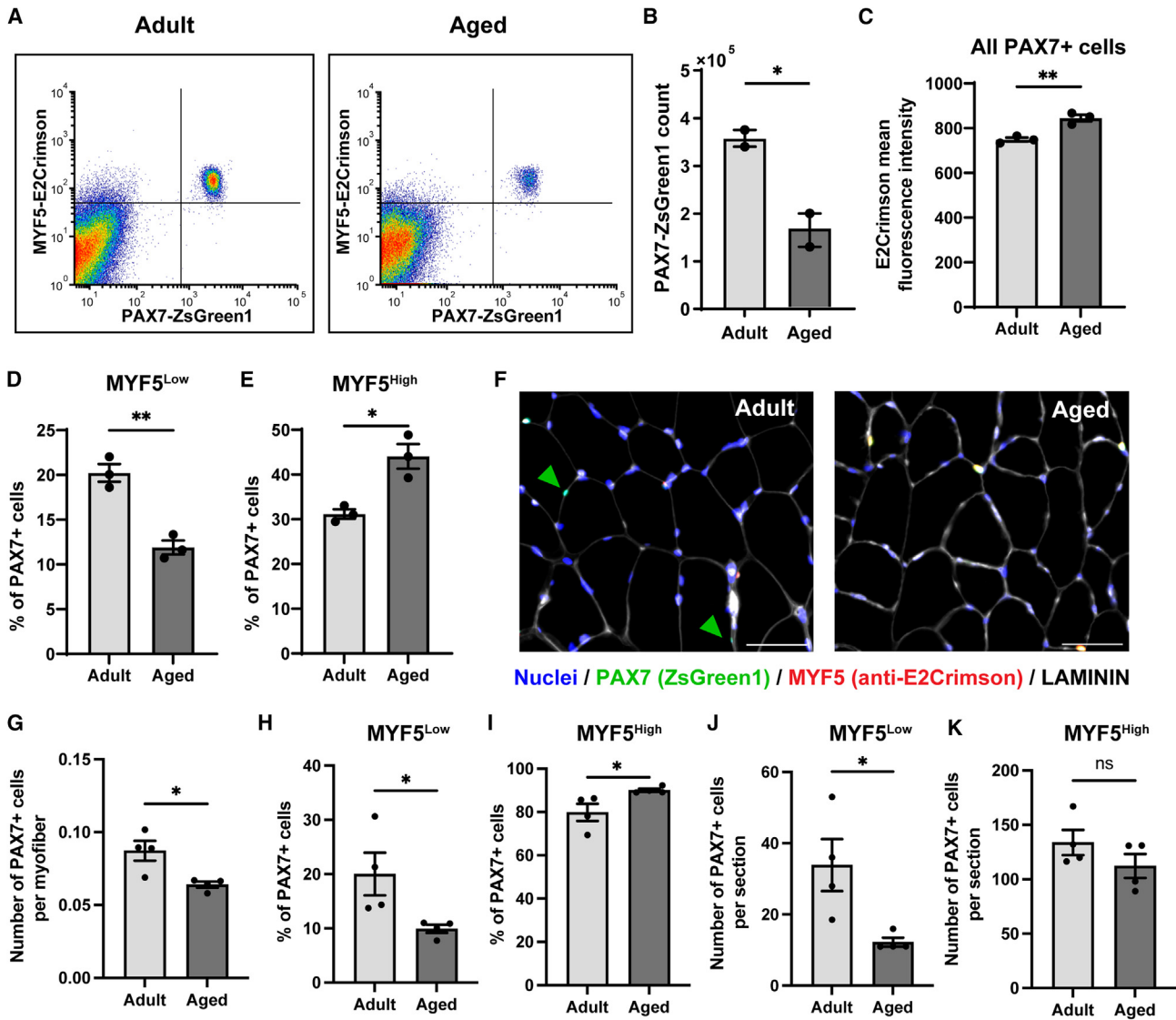


**Figure 7. Aging primarily affects MYF5<sup>Low</sup> MuSCs**

(A) Representative flow cytometry profiles of MuSCs isolated from adult (4 m.o., left) and aged (22 m.o., right) StemRep mice.

(B) Flow cytometry-based quantification of MuSC numbers in adult and aged StemRep mice.  $n = 4$  mice, 2 pools of 2 mice.

(C) Quantification of MYF5-E2Crimson mean fluorescence intensity in MuSCs derived from adult and aged StemRep mice.

(D and E) Proportion of MYF5<sup>Low</sup> (D) and MYF5<sup>High</sup> (E) MuSCs in adult and aged StemRep mice.  $n = 3$  mice per group, each datapoint represents one mouse.

(F–K) Representative images (F) and quantification of total PAX7 positive cells (G), proportion, and absolute numbers of MYF5<sup>Low</sup> (H, J) and MYF5<sup>High</sup> (I, K) cells on uninjured *tibialis anterior* cross-sections from adult and aged StemRep mice.  $n = 4$  mice, each datapoint represents one mouse. Scale bar, 50  $\mu\text{m}$ . Data presented are means  $\pm$  SEM. \* $p < 0.05$ , \*\* $p < 0.01$  in a two-tailed unpaired Student's *t* test for each population (B, C, D, E, G, H, I, J, K).

the temporal endogenous expression patterns of PAX7 and MYF5 (Bentzinger et al., 2012). Although both MYF5<sup>Low</sup> and MYF5<sup>High</sup> MuSCs isolated from StemRep mice were equally capable of forming stem cell colonies and myotubes, MYF5<sup>Low</sup> cells were slower to enter cell cycle, proliferate, and commit to myogenic differentiation, demonstrating that

this subpopulation resides in a deeper state of quiescence compared to MYF5<sup>High</sup> cells. This observation was supported by molecular analyses of the MYF5 subpopulations, showing that MYF5<sup>High</sup> cells are enriched in transcripts implicated in early activation whereas MYF5<sup>Low</sup> MuSCs expressed higher levels of canonical quiescence markers.



About 20% of MYF5<sup>Low</sup> MuSCs in StemRep mice are present in adult homeostatic muscle and persist throughout regenerative myogenesis, which aligns with the finding that cells with only one genomic copy of *Myf5* have a higher self-renewal capacity and engraft better than MuSCs with two copies of *Myf5* (Gayraud-Morel et al., 2012). Similarly, a subpopulation of asymmetrically self-renewing MYF5-lineage-negative satellite stem cells was also found in *Myf5*-Cre; ROSA26-YFP mice (Kuang et al., 2007). Furthermore, previous work has identified a subset of PAX7-positive MuSCs that is able to downregulate MYOD and withdraw from the cell cycle following activation (Zammit et al., 2004). It has been suggested that this represents a mechanism to generate “reserve cells” that are set aside for subsequent rounds of injury and repair. These data further support the idea that MYF5<sup>Low</sup> cells with their inherent capacity for asymmetric segregation of MYOD along with slower activation and cycling kinetics, and increased quiescence features, play an important role in maintaining the MuSC pool. We also observed that MYF5<sup>Low</sup> cells with high self-renewal capacity through asymmetric division contain significantly increased levels of PAX7 protein, which represents a notable parallel with the PAX7-nGFP<sup>Hi</sup> subpopulation observed in mice with a nuclear GFP inserted into the first exon of *Pax7* gene that was shown to undergo asymmetric DNA strand segregation (Rocheteau et al., 2012). The discovery that MYF5<sup>Low</sup> MuSCs are residing in deep quiescence is yet another common denominator with previous studies describing superior stemness characteristics of the most dormant stem cell populations in skeletal muscle (Garcia-Prat et al., 2020; Rocheteau et al., 2012; Rodgers et al., 2014). Here, we present the unifying hypothesis that adult skeletal muscle contains a singular subpopulation of MuSCs with superior stem cell character and self-renewal capacity that resides in deep quiescence and is characterized by high levels of PAX7 and low levels of myogenic commitment factors such as MYF5 and MYOD. This population of cells likely plays a central role in maintaining the stem cell pool and the regenerative capacity of skeletal muscle.

To demonstrate a specific application of StemRep mice in studying physiological changes, we examined the influence of age on the MYF5<sup>Low</sup> and MYF5<sup>High</sup> MuSC subpopulations. When compared to adult 4 m.o. StemRep mice, aged 24 m.o. StemRep mice showed higher levels of MYF5 across the entire MuSC population. Aging also specifically reduced the amount of MYF5<sup>Low</sup> MuSCs, supporting the model that aging causes a break of MuSC quiescence which impairs maintenance of the uncommitted stem cell pool and ultimately contributes to regenerative failure (Ancel et al., 2021; Brack et al., 2007). Next to aging, an impaired healing capacity of skeletal muscle has been described to accompany many other conditions, including muscular dystrophy and cancer cachexia (Deprez et al.,

2023; Mashinchian et al., 2018). Therefore, future experiments using the StemRep alleles on disease backgrounds may provide important novel insights into pathogenesis and might unravel therapeutic approaches to target specific MuSC subpopulations.

Our study draws several important parallels with previous work, fills in long-standing gaps in our understanding of MuSC subpopulations, and establishes the StemRep line as a novel tool for the interrogation of stem cell heterogeneity in skeletal muscle. Our results unify multiple existing theories about the quintessential stem cell population in skeletal muscle and point toward a fraction of roughly 20% of MuSCs that reside in deep quiescence and are marked by high PAX7 and low MYF5 protein levels. The broad availability of StemRep mice to the field will enable future in-depth studies addressing the molecular characteristics of this MuSC population in health and disease.

## EXPERIMENTAL PROCEDURES

### Resources availability

#### Lead contact

Further information and requests for resources and reagents should be directed to and will be fulfilled by the lead contact, Pascal Stuelsatz ([pascal.stuelsatz@rd.nestle.com](mailto:pascal.stuelsatz@rd.nestle.com)).

#### Materials availability

The newly generated StemRep mice could be available from the investigators and distributed by Taconic Biosciences. All softwares used were freely or commercially available. Any additional information required to reanalyze the data reported in this paper is available upon justified request to the corresponding author. Other materials are available upon justified request within the limits of non-renewable materials.

#### Data and code availability

RNA sequencing data have been deposited to Gene Expression Omnibus under accession number GEO: GSE207321.

### Animal housing and ethics

All *in vivo* experiments and protocols were performed in compliance with the regulations of the Swiss Animal Experimentation Ordinance and approved by the internal ethics committee of Nestlé Research and the ethical committee of the canton de Vaud under license VD3331. Mice were housed under standard conditions (up to 5 mice per cage) and allowed access to food and water *ad libitum*. Unless otherwise specified, all experiments were conducted using both males and females at an approx. 1:1 ratio. All data were systematically analyzed for sex differences and the results were reported if divergence was observed. For aging studies, animals were bred and housed in the same facility using housing conditions described previously.

### Isolation of MYF5 subpopulations by FACS

MuSCs from StemRep mice were isolated as previously described (Lukjanenko et al., 2016). Hindlimb muscles from injured or uninjured mice were collected, minced, and digested with Dispase II



(2.5 U/mL) (Roche), Collagenase B (0.2%) (Roche), and MgCl<sub>2</sub> (5 mM) at 37°C. The preparation was then filtered sequentially through 100 micron and 30 micron filters. For initial validation of the PAX7/MYF5 model, cells were incubated at 4°C for 30 min with antibodies against CD45 (Invitrogen, #MCD4528, 1/25), CD31 (Invitrogen, #RM5228, 1/25), CD11b (Invitrogen, #RM2828, 1/25), CD34 (BD Biosciences, #560238, 1/60), Ly-6A/E (BD Biosciences, #561021, 1/150), and ITGA7 (R&D Systems, #FAB3518N, 1/30). MYF5 subpopulations identified as PAX7-ZsGreen1 positive and MYF5-E2Crimson high or low were isolated using a Beckman Coulter Astrios cell sorter.

### Muscle regeneration

Muscle regeneration was induced by intramuscular injection of 25, 50, and 50 µL of 20 µM cardiotoxin (Latoxan) into the TA, *gastrocnemius* (GC), and *quadriceps femoris* (QD) muscles, respectively, under a short anesthesia using 2% isoflurane. For analgesia, buprenorphine was administered at a dosage of 0.1 mg/kg subcutaneously before the intramuscular injection followed by a second dose 24 h after. Mice were sacrificed by CO<sub>2</sub> exposure 3, 7, 14, or 21 days post-injury and muscles were collected for analysis. TA muscles were mounted on 6% traga-canth gum (Sigma, #G1128) and frozen in isopentane (Sigma, #M32631) cooled with liquid nitrogen for histological analysis. GC and QD muscles were immediately processed after harvest for analysis by flow cytometry.

### Cell cycle analysis of MYF5 subpopulations by flow cytometry

To facilitate identification of different phases of cell cycle, MuSCs from StemRep mice were stained with Hoechst 33342 (Sigma, #B2261) and Pyronin Y (Sigma, #P9172). After isolation, MuSCs are resuspended in 1 mL of growing medium (DMEM with 20% heat-inactivated FBS, 10% horse serum, 2.5 ng/mL bFGF, 1% P/S, and 1% L-glutamine) containing 10 µg/mL of Hoechst 33342. Cells were incubated at 37°C in an incubator for 45 min. After this incubation period, Pyronin Y was directly added to a final concentration of 100 µg/mL and incubation continued at 37°C for additional 15 min. The cells were then analyzed using an LSR Fortessa (Becton Dickinson).

### Histology and image analysis

Frozen TA muscles were sectioned at 10 µm with a cryostat (Leica Biosystems). Samples were fixed with 4% PFA (EMS, #157-4-100) and permeabilized in 0.5% Triton X-100 (Sigma, X100) diluted in PBS (PBTX). Sections were further blocked in 4% BSA for 2 h. For immunostaining, the slides were incubated with primary antibodies anti-E2Crimson (Takara Bio, #632496, 1/1,000), anti-PAX7 (purified hybridoma, DSHB, 1/200), and anti-Laminin (LSBio, #LS-C96142, 1/1,000). Nuclei were labeled with Hoechst 33342 (Sigma, #B2261) during secondary antibody incubation (Thermo Fisher Scientific, #A21245 and #A21437). Slides were then mounted using Dako fluorescent mounting medium (Agilent, #S302380-2) and imaged with the Olympus VS120 and VS200 slide scanner. Images were analyzed using the VS-ASW FL software measurement tool. The number of PAX7- and MYF5-positive cells was determined by manually counting injured areas on muscle sections.

To access the expression of PAX7 and MYF5 in quiescence during homeostasis, Qupath, an open-source image analytical software, was used to annotate define region of interest (ROI) (Bankhead et al., 2017). First, tissue area and fibers were automatically identified according to LAMININ segmentation. Then, MuSCs were detected as areas of staining above the background level by applying intensity thresholds for the labeled proteins within ROI. Annotation measurements were exported, and information on size, number, intensity features, and numbers of positive cells was obtained per image.

### MuSC-derived myoblasts and staining

FACS-isolated MYF5<sup>High</sup> and MYF5<sup>Low</sup> cells were directly plated onto 0.2% gelatin-coated 384-well plates in growth medium (DMEM supplemented with 20% heat-inactivated FBS, 10% horse serum, 2.5 ng/mL bFGF, 1% P/S and 1% L-glutamine). To assess proliferation, 5 µM EdU was added in the medium for 2 h prior to the assessed time points. EdU incorporation was revealed using the Click-iT assay (Thermo Fisher Scientific, #C10338) according to manufacturer's instructions. Briefly, cells were fixed during 15 min in 4% PFA, permeabilized during 20 min in PBTX 0.5%, stained with the Click-iT reaction mix, and counterstained with Hoechst 33342 (Sigma, #B2261). To assess differentiation, 5,000 MYF5<sup>High</sup> and MYF5<sup>Low</sup> cells were seeded onto 0.2% gelatin-coated 384-well plates in growing medium. 12 h post-plating, cells were switched to differentiating conditions (DMEM with 5% horse serum and 1% P/S) and fixed after 4 days. To track MuSC fate over time, 1,000 ZsGreen1-positive cells were seeded onto 0.2% gelatin-coated 384-well plates in growing medium. Cells were grown for 5 days in growth medium. MuSC differentiation was induced after five days of growth, by switching to differentiation medium for 2 days. Immunostaining was performed by blocking for 1 h in 4% BSA (Sigma, #A8022) and staining with anti-dsRed (Takara Bio, #632496, 1/1,000), anti-PAX7 (purified hybridoma, DSHB, 1/1,000), anti-MYOD (LSBio, #LS-C143580-100, 1/500), anti-Myogenin (Abcam, #124800, 1/500), or anti-MyHC (Merck, #05-716, 1/200) and then with appropriate secondary antibodies (Thermo Fisher Scientific, #A21245 and #A32727) and Hoechst 33342 (Sigma, #B2261). Images were acquired using the ImageXpress (Molecular Devices) platform and quantifications were performed using the MetaXpress software (Molecular Devices). Exclusion of staining artifacts was performed based on morphological analysis and myotubes were detected based on the segmentation of MyHC staining. Multi-wavelength cell scoring was performed by identifying positive and negative populations based on a minimum intensity threshold for each marker using an automated image processing module.

To identify asymmetric and symmetric divisions, MYOD was used as a segregation marker. Images from MuSC *ex vivo* culture at 18 and 36 h were analyzed. Cell divisions were manually detected by tracking a pair of cells or a cluster of cells in close proximity. Then, thresholding detection was applied to generate a classifier and extract features for every staining combination due to fluorescence channel dependency. A cutoff was applied based on the intensity of MYOD staining, to classify each cell division as symmetric (MYOD in both daughter cells) or asymmetric (MYOD only in one daughter cells).



## qPCR of quiescence genes on MYF5 subpopulations

Freshly isolated MYF5<sup>High</sup> and MYF5<sup>Low</sup> cells from 4 adult male individual mice. Each sample was processed as a biological replicate. Cell pellets were lysed with RLT buffer containing beta-mercaptoethanol and cooled down at  $-80^{\circ}\text{C}$ . RNA was extracted using Micro RNeasy Kit (QIAGEN, # 74004) following supplier's instructions. RNA samples were subjected to reverse transcription using random primers from High-Capacity cDNA Reverse Transcription Kit (Thermo Fisher Scientific, #4368814). Quantitative PCR on MuSC was performed using Master Mix for TaqMan Universal PCR (Thermo Fisher Scientific, #4305719) on a LightCycler 480 (Roche) and the following probes were used: *Cd34*: Mm00519283\_m1, *Cxcr4*: Mm01996749\_s1, *Calcr*: Mm00432282\_m1, *Pax7*: Mm01354484\_m1, and *Gapdh*: Mm99999915\_g1.

## RNA sequencing of MYF5<sup>High</sup> and MYF5<sup>Low</sup> subpopulations

MYF5<sup>High</sup> and MYF5<sup>Low</sup> MuSCs were isolated from a pool of 4 male and 4 female mice and repeated in two independent experiments, and total RNA was extracted using Agencourt RNAdvance Tissue Kit (Beckman Coulter, #A32646) with a quality score of RQN 9.3 to 10. Libraries were constructed from cDNA generated and amplified (21 cycles) from 20 ng of RNA, following the user guide with QuantSeq 3' mRNA-Seq Library Prep Kit FWD for Illumina (Lexogen) without any modification. Libraries were quantified with Quant-iT Picogreen (Invitrogen, #10545213). The library sizes were controlled with the High Sensitivity NGS Fragment Analysis Kit on a Fragment Analyzer (Agilent). Sequencing was performed on HiSeq 2500 with Rapid V2 chemistry SR 65 cycles (Illumina) using two different flow cells loaded at 2 pM and with 3% Phix. Primary data quality control was performed during the sequencing run to ensure the optimal flow cell loading (cluster density) and check the quality metrics of the sequencing run.

## Statistical analyses

Unless otherwise stated, data were analyzed using the Prism 9 software package and represented as mean  $\pm$  standard error to the mean (SEM). The SEM represents the precision of the mean estimate and indicates the uncertainty associated with the sample mean. In our case, the larger SEM reflects the inherent variability and potential sampling error due to the relatively small sample size ( $n = 4$ ). To correct this limitation, we also included a supplementary table summarizing the average values of all graphs and the respective standard deviations, as well as the confidence intervals (Table S1). Readouts used in this study were assessed for normality based on the distribution of historical values across multiple experiments using a D'Agostino-Pearson test. Two conditions comparisons were analyzed using a Student's *t* test.

## SUPPLEMENTAL INFORMATION

Supplemental information can be found online at <https://doi.org/10.1016/j.stemcr.2024.05.005>.

## ACKNOWLEDGMENTS

We thank the NIHS community for critical discussions of the results and manuscript. The project was funded by Nestlé Research.

C.F.B. was supported by the Canadian Institutes of Health Research (CIHR, PJT-162442), the Natural Sciences and Engineering Research Council of Canada (NSERC, RGPIN-2017-05490), the Fonds de Recherche du Québec - Santé (FRQS, Dossiers 296357, 34813, and 36789), the Fonds de Recherche du Québec - Nature et Technologies (FRQNT, Dossier 331297), the Canadian Stem Cell Network, and a research chair of the Centre de Recherche Médicale de l'Université de Sherbrooke (CRMUS). S.C.S. was supported by a postdoctoral fellowship by the German Research Foundation (DFG, 505064275).

## AUTHOR CONTRIBUTIONS

S.A., J.M., P.S., and J.N.F. designed the experimental strategy, interpreted the results, and wrote the manuscript. P.S. and J.N.F. led the project. C.F.B. ideated and conceived the mouse line and edited the manuscript. S.A., J.M., F.S., S.K., S.C.S., and P.S. performed the experiments and analyzed the data. S.A., F.S., L.T., M.O., and G.D. designed the flow cytometry strategy, performed the sorts, and analyzed the results. J.L.S.-G. supported animal work. E.M. analyzed transcriptomic experiments. G.J. and S.M. supported imaging and genomics. All authors reviewed the manuscript.

## DECLARATION OF INTERESTS

Except S.C.S., all authors are or were employees of Société des Produits Nestlé SA.

Received: June 27, 2023

Revised: May 13, 2024

Accepted: May 14, 2024

Published: June 13, 2024

## REFERENCES

- Ancel, S., Stuelsatz, P., and Feige, J.N. (2021). Muscle Stem Cell Quiescence: Controlling Stemness by Staying Asleep. *Trends Cell Biol.* *31*, 556–568. <https://doi.org/10.1016/j.tcb.2021.02.006>.
- Bachman, J.F., Klose, A., Liu, W., Paris, N.D., Blanc, R.S., Schmalz, M., Knapp, E., and Chakkalakal, J.V. (2018). Prepubertal skeletal muscle growth requires Pax7-expressing satellite cell-derived myonuclear contribution. *Development* *145*, dev167197. <https://doi.org/10.1242/dev.167197>.
- Bankhead, P., Loughrey, M.B., Fernández, J.A., Dombrowski, Y., McArt, D.G., Dunne, P.D., McQuaid, S., Gray, R.T., Murray, L.J., Coleman, H.G., et al. (2017). QuPath: Open source software for digital pathology image analysis. *Sci. Rep.* *7*, 16878. <https://doi.org/10.1038/s41598-017-17204-5>.
- Beauchamp, J.R., Heslop, L., Yu, D.S., Tajbakhsh, S., Kelly, R.G., Wernig, A., Buckingham, M.E., Partridge, T.A., and Zammit, P.S. (2000). Expression of CD34 and Myf5 defines the majority of quiescent adult skeletal muscle satellite cells. *J. Cell Biol.* *151*, 1221–1234. <https://doi.org/10.1083/jcb.151.6.1221>.
- Bentzinger, C.F., Wang, Y.X., and Rudnicki, M.A. (2012). Building muscle: molecular regulation of myogenesis. *Cold Spring Harbor Perspect. Biol.* *4*, a008342. <https://doi.org/10.1101/cshperspect.a008342>.



- Brack, A.S., Conboy, M.J., Roy, S., Lee, M., Kuo, C.J., Keller, C., and Rando, T.A. (2007). Increased Wnt signaling during aging alters muscle stem cell fate and increases fibrosis. *Science* 317, 807–810. <https://doi.org/10.1126/science.1144090>.
- Brizzard, B. (2008). Epitope tagging. *Biotechniques* 44, 693–695. <https://doi.org/10.2144/000112841>.
- Cheung, T.H., and Rando, T.A. (2013). Molecular regulation of stem cell quiescence. *Nat. Rev. Mol. Cell Biol.* 14, 329–340. <https://doi.org/10.1038/nrm3591>.
- Crist, C.G., Montarras, D., and Buckingham, M. (2012). Muscle satellite cells are primed for myogenesis but maintain quiescence with sequestration of Myf5 mRNA targeted by microRNA-31 in mRNP granules. *Cell Stem Cell* 11, 118–126. <https://doi.org/10.1016/j.stem.2012.03.011>.
- Deprez, A., Orfi, Z., Rieger, L., and Dumont, N.A. (2023). Impaired muscle stem cell function and abnormal myogenesis in acquired myopathies. *Biosci. Rep.* 43, BSR20220284. <https://doi.org/10.1042/BSR20220284>.
- Der Vartanian, A., Quéting, M., Michineau, S., Auradé, F., Hayashi, S., Dubois, C., Rocancourt, D., Drayton-Libotte, B., Szegedi, A., Buckingham, M., et al. (2019). PAX3 Confers Functional Heterogeneity in Skeletal Muscle Stem Cell Responses to Environmental Stress. *Cell Stem Cell* 24, 958–973.e9. <https://doi.org/10.1016/j.stem.2019.03.019>.
- Donnelly, M.L.L., Hughes, L.E., Luke, G., Mendoza, H., Ten Dam, E., Gani, D., and Ryan, M.D. (2001). The “cleavage” activities of foot-and-mouth disease virus 2A site-directed mutants and naturally occurring “2A-like” sequences. *J. Gen. Virol.* 82, 1027–1041. <https://doi.org/10.1099/0022-1317-82-5-1027>.
- Dumont, N.A., Wang, Y.X., and Rudnicki, M.A. (2015). Intrinsic and extrinsic mechanisms regulating satellite cell function. *Development* 142, 1572–1581. <https://doi.org/10.1242/dev.114223>.
- Englund, D.A., Murach, K.A., Dungan, C.M., Figueiredo, V.C., Vecchetti, I.J., Dupont-Versteegden, E.E., McCarthy, J.J., and Peterson, C.A. (2020). Depletion of resident muscle stem cells negatively impacts running volume, physical function, and muscle fiber hypertrophy in response to lifelong physical activity. *Am. J. Physiol. Cell Physiol.* 318, C1178–c1188. <https://doi.org/10.1152/ajpcell.00090.2020>.
- Fukada, S.i., Uezumi, A., Ikemoto, M., Masuda, S., Segawa, M., Tanimura, N., Yamamoto, H., Miyagoe-Suzuki, Y., and Takeda, S. (2007). Molecular signature of quiescent satellite cells in adult skeletal muscle. *Stem Cell.* 25, 2448–2459. <https://doi.org/10.1634/stemcells.2007-0019>.
- García-Prat, L., Perdiguero, E., Alonso-Martín, S., Dell’Orso, S., Ravichandran, S., Brooks, S.R., Juan, A.H., Campanario, S., Jiang, K., Hong, X., et al. (2020). FoxO maintains a genuine muscle stem cell quiescent state until geriatric age. *Nat. Cell Biol.* 22, 1307–1318. <https://doi.org/10.1038/s41556-020-00593-7>.
- Gayraud-Morel, B., Chrétien, F., Jory, A., Sambasivan, R., Negroni, E., Flamant, P., Soubigou, G., Coppée, J.Y., Di Santo, J., Cumanò, A., et al. (2012). Myf5 haploinsufficiency reveals distinct cell fate potentials for adult skeletal muscle stem cells. *J. Cell Sci.* 125, 1738–1749. <https://doi.org/10.1242/jcs.097006>.
- Hennecke, M., Kwissa, M., Metzger, K., Oumard, A., Kröger, A., Schirmbeck, R., Reimann, J., and Hauser, H. (2001). Composition and arrangement of genes define the strength of IRES-driven translation in bicistronic mRNAs. *Nucleic Acids Res.* 29, 3327–3334. <https://doi.org/10.1093/nar/29.16.3327>.
- Kassar-Duchossoy, L., Gayraud-Morel, B., Gomès, D., Rocancourt, D., Buckingham, M., Shinin, V., and Tajbakhsh, S. (2004). Mrf4 determines skeletal muscle identity in Myf5:Myod double-mutant mice. *Nature* 431, 466–471. <https://doi.org/10.1038/nature02876>.
- Kawakami, A., Kimura-Kawakami, M., Nomura, T., and Fujisawa, H. (1997). Distributions of PAX6 and PAX7 proteins suggest their involvement in both early and late phases of chick brain development. *Mech. Dev.* 66, 119–130. [https://doi.org/10.1016/s0925-4773\(97\)00097-x](https://doi.org/10.1016/s0925-4773(97)00097-x).
- Kim, J.H., Lee, S.-R., Li, L.-H., Park, H.-J., Park, J.-H., Lee, K.Y., Kim, M.-K., Shin, B.A., and Choi, S.-Y. (2011). High cleavage efficiency of a 2A peptide derived from porcine teschovirus-1 in human cell lines, zebrafish and mice. *PLoS One* 6, e18556. <https://doi.org/10.1371/journal.pone.0018556>.
- Kuang, S., Kuroda, K., Le Grand, F., and Rudnicki, M.A. (2007). Asymmetric self-renewal and commitment of satellite stem cells in muscle. *Cell* 129, 999–1010. <https://doi.org/10.1016/j.cell.2007.03.044>.
- Lepper, C., Partridge, T.A., and Fan, C.M. (2011). An absolute requirement for Pax7-positive satellite cells in acute injury-induced skeletal muscle regeneration. *Development* 138, 3639–3646. <https://doi.org/10.1242/dev.067595>.
- Liu, Z., Chen, O., Wall, J.B.J., Zheng, M., Zhou, Y., Wang, L., Vaseghi, H.R., Qian, L., and Liu, J. (2017). Systematic comparison of 2A peptides for cloning multi-genes in a polycistronic vector. *Sci. Rep.* 7, 2193. <https://doi.org/10.1038/s41598-017-02460-2>.
- Luke, G.A., de Felipe, P., Lukashev, A., Kallioinen, S.E., Bruno, E.A., and Ryan, M.D. (2008). Occurrence, function and evolutionary origins of “2A-like” sequences in virus genomes. *J. Gen. Virol.* 89, 1036–1042. <https://doi.org/10.1099/vir.0.83428-0>.
- Lukjanenko, L., Jung, M.J., Hegde, N., Perruisseau-Carrier, C., Migliavacca, E., Rozo, M., Karaz, S., Jacot, G., Schmidt, M., Li, L., et al. (2016). Loss of fibronectin from the aged stem cell niche affects the regenerative capacity of skeletal muscle in mice. *Nat. Med.* 22, 897–905. <https://doi.org/10.1038/nm.4126>.
- Machado, L., Esteves de Lima, J., Fabre, O., Proux, C., Legendre, R., Szegedi, A., Varet, H., Ingerslev, L.R., Barrès, R., Relaix, F., and Mourikis, P. (2017). In Situ Fixation Redefines Quiescence and Early Activation of Skeletal Muscle Stem Cells. *Cell Rep.* 21, 1982–1993. <https://doi.org/10.1016/j.celrep.2017.10.080>.
- Maesner, C.C., Almada, A.E., and Wagers, A.J. (2016). Established cell surface markers efficiently isolate highly overlapping populations of skeletal muscle satellite cells by fluorescence-activated cell sorting. *Skeletal Muscle* 6, 35. <https://doi.org/10.1186/s13395-016-0106-6>.
- Mahato, R.I., Smith, L.C., and Rolland, A. (1999). 4 - Pharmaceutical Perspectives of Nonviral Gene Therapy. In *Advances in Genetics*, J.C. Hall, J.C. Dunlap, T. Friedmann, and F. Giannelli, eds. (Academic Press), pp. 95–156.



- von Maltzahn, J., Jones, A.E., Parks, R.J., and Rudnicki, M.A. (2013). Pax7 is critical for the normal function of satellite cells in adult skeletal muscle. *Proc. Natl. Acad. Sci. USA* *110*, 16474–16479. <https://doi.org/10.1073/pnas.1307680110>.
- Mashinchian, O., Pisconti, A., Le Moal, E., and Bentzinger, C.F. (2018). The Muscle Stem Cell Niche in Health and Disease. *Curr. Top. Dev. Biol.* *126*, 23–65. <https://doi.org/10.1016/bs.ctdb.2017.08.003>.
- Matz, M.V., Fradkov, A.F., Labas, Y.A., Savitsky, A.P., Zarskiy, A.G., Markelov, M.L., and Lukyanov, S.A. (1999). Fluorescent proteins from nonbioluminescent Anthozoa species. *Nat. Biotechnol.* *17*, 969–973. <https://doi.org/10.1038/13657>.
- Mauro, A. (1961). Satellite cell of skeletal muscle fibers. *J. Biophys. Biochem. Cytol.* *9*, 493–495. <https://doi.org/10.1083/jcb.9.2.493>.
- McKinnell, I.W., Ishibashi, J., Le Grand, F., Punch, V.G.J., Addicks, G.C., Greenblatt, J.F., Dilworth, F.J., and Rudnicki, M.A. (2008). Pax7 activates myogenic genes by recruitment of a histone methyltransferase complex. *Nat. Cell Biol.* *10*, 77–84. <https://doi.org/10.1038/ncb1671>.
- Morrill, S.A., and Amon, A. (2019). Why haploinsufficiency persists. *Proc. Natl. Acad. Sci. USA* *116*, 11866–11871. <https://doi.org/10.1073/pnas.1900437116>.
- Olguin, H.C., and Olwin, B.B. (2004). Pax-7 up-regulation inhibits myogenesis and cell cycle progression in satellite cells: a potential mechanism for self-renewal. *Dev. Biol.* *275*, 375–388. <https://doi.org/10.1016/j.ydbio.2004.08.015>.
- Porpiglia, E., Samusik, N., Ho, A.T.V., Cosgrove, B.D., Mai, T., Davis, K.L., Jager, A., Nolan, G.P., Bendall, S.C., Fantl, W.J., and Blau, H.M. (2017). High-resolution myogenic lineage mapping by single-cell mass cytometry. *Nat. Cell Biol.* *19*, 558–567. <https://doi.org/10.1038/ncb3507>.
- Rocheteau, P., Gayraud-Morel, B., Siegl-Cachedenier, I., Blasco, M.A., and Tajbakhsh, S. (2012). A subpopulation of adult skeletal muscle stem cells retains all template DNA strands after cell division. *Cell* *148*, 112–125. <https://doi.org/10.1016/j.cell.2011.11.049>.
- Rodgers, J.T., King, K.Y., Brett, J.O., Cromie, M.J., Charville, G.W., Maguire, K.K., Brunson, C., Mastey, N., Liu, L., Tsai, C.R., et al. (2014). mTORC1 controls the adaptive transition of quiescent stem cells from G0 to G(Alert). *Nature* *510*, 393–396. <https://doi.org/10.1038/nature13255>.
- Sambasivan, R., Yao, R., Kissenpfennig, A., Van Wittenberghe, L., Paldi, A., Gayraud-Morel, B., Guenou, H., Malissen, B., Tajbakhsh, S., and Galy, A. (2011). Pax7-expressing satellite cells are indispensable for adult skeletal muscle regeneration. *Development* *138*, 3647–3656. <https://doi.org/10.1242/dev.067587>.
- Scaramozza, A., Park, D., Kollu, S., Beerman, I., Sun, X., Rossi, D.J., Lin, C.P., Scadden, D.T., Crist, C., and Brack, A.S. (2019). Lineage Tracing Reveals a Subset of Reserve Muscle Stem Cells Capable of Clonal Expansion under Stress. *Cell Stem Cell* *24*, 944–957.e5. <https://doi.org/10.1016/j.stem.2019.03.020>.
- Schmidt, M., Schüler, S.C., Hüttner, S.S., von Eyss, B., and von Maltzahn, J. (2019). Adult stem cells at work: regenerating skeletal muscle. *Cell. Mol. Life Sci.* *76*, 2559–2570. <https://doi.org/10.1007/s00018-019-03093-6>.
- Schüler, S.C., Liu, Y., Dumontier, S., Grandbois, M., Le Moal, E., Cornelison, D., and Bentzinger, C.F. (2022). Extracellular matrix: Brick and mortar in the skeletal muscle stem cell niche. *Front. Cell Dev. Biol.* *10*, 1056523. <https://doi.org/10.3389/fcell.2022.1056523>.
- Seale, P., Sabourin, L.A., Giris-Gabardo, A., Mansouri, A., Gruss, P., and Rudnicki, M.A. (2000). Pax7 is required for the specification of myogenic satellite cells. *Cell* *102*, 777–786. [https://doi.org/10.1016/s0092-8674\(00\)00066-0](https://doi.org/10.1016/s0092-8674(00)00066-0).
- Shyu, A.-B., Wilkinson, M.F., and van Hoof, A. (2008). Messenger RNA regulation: to translate or to degrade. *EMBO J.* *27*, 471–481. <https://doi.org/10.1038/sj.emboj.7601977>.
- Sousa-Victor, P., García-Prat, L., and Muñoz-Cánoves, P. (2022). Control of satellite cell function in muscle regeneration and its disruption in ageing. *Nat. Rev. Mol. Cell Biol.* *23*, 204–226. <https://doi.org/10.1038/s41580-021-00421-2>.
- Strack, R.L., Hein, B., Bhattacharyya, D., Hell, S.W., Keenan, R.J., and Glick, B.S. (2009). A rapidly maturing far-red derivative of DsRed-Express2 for whole-cell labeling. *Biochemistry* *48*, 8279–8281. <https://doi.org/10.1021/bi900870u>.
- Szymczak, A.L., Workman, C.J., Wang, Y., Vignali, K.M., Dilioglou, S., Vanin, E.F., and Vignali, D.A.A. (2004). Correction of multi-gene deficiency *in vivo* using a single “self-cleaving” 2A peptide-based retroviral vector. *Nat. Biotechnol.* *22*, 589–594. <https://doi.org/10.1038/nbt957>.
- Tajbakhsh, S., Rocancourt, D., and Buckingham, M. (1996). Muscle progenitor cells failing to respond to positional cues adopt non-myogenic fates in myf-5 null mice. *Nature* *384*, 266–270. <https://doi.org/10.1038/384266a0>.
- van Velthoven, C.T.J., and Rando, T.A. (2019). Stem Cell Quiescence: Dynamism, Restraint, and Cellular Idling. *Cell Stem Cell* *24*, 213–225. <https://doi.org/10.1016/j.stem.2019.01.001>.
- van Velthoven, C.T.J., de Morree, A., Egner, I.M., Brett, J.O., and Rando, T.A. (2017). Transcriptional Profiling of Quiescent Muscle Stem Cells *In Vivo*. *Cell Rep.* *21*, 1994–2004. <https://doi.org/10.1016/j.celrep.2017.10.037>.
- Zammit, P.S. (2017). Function of the myogenic regulatory factors Myf5, MyoD, Myogenin and MRF4 in skeletal muscle, satellite cells and regenerative myogenesis. *Semin. Cell Dev. Biol.* *72*, 19–32. <https://doi.org/10.1016/j.semcdb.2017.11.011>.
- Zammit, P.S., Golding, J.P., Nagata, Y., Hudon, V., Partridge, T.A., and Beauchamp, J.R. (2004). Muscle satellite cells adopt divergent fates. *J. Cell Biol.* *166*, 347–357. <https://doi.org/10.1083/jcb.200312007>.
- Zismanov, V., Chichkov, V., Colangelo, V., Jamet, S., Wang, S., Syme, A., Koromilas, A.E., and Crist, C. (2016). Phosphorylation of eIF2 $\alpha$  Is a Translational Control Mechanism Regulating Muscle Stem Cell Quiescence and Self-Renewal. *Cell Stem Cell* *18*, 79–90. <https://doi.org/10.1016/j.stem.2015.09.020>.